

UAVGENT: A Language-Guided Distributed Control Framework

Ziyi Zhang* and Xiyu Deng* and Guannan Qu and Yorie Nakahira

Department of Electrical and Computer Engineering

Carnegie Mellon University

5000 Forbes Avenue, Pittsburgh, PA 15213

ziyizhan, xiyud, gqu, ynakahira@andrew.cmu.edu

Abstract

We study language-in-the-loop control for multi-drone systems that execute evolving, high-level missions while retaining formal robustness guarantees at the physical layer. We propose a three-layer architecture in which (i) a human operator issues natural-language instructions, (ii) an LLM-based supervisor periodically interprets, verifies, and corrects the commanded task in the context of the latest state and target estimates, and (iii) a distributed inner-loop controller tracks the resulting reference using only local relative information. We derive a theoretical guarantee that characterizes tracking performance under bounded disturbances and piecewise-smooth references with discrete jumps induced by LLM updates. Overall, our results illustrate how centralized language-based task reasoning can be combined with distributed feedback control to achieve complex behaviors with provable robustness and stability.

1 Introduction

Multi-robot systems are increasingly deployed for surveillance, inspection, environmental monitoring, and emergency response (Queraltà et al., 2020). Yet specifying and adjusting multi-agent behavior in dynamic environments can be both challenging and tedious, even for an expert user, as it requires not only relevant domain knowledge to determine the optimal action but also rapid adaptation to an evolving environment. The above problem magnifies when the number of drones increases, as designing control policies for each drone and having them collaborate in a time-varying environment requires designing and modifying many parameters that may be prohibitive for any single individual.

The development of natural language interfaces offers an approach to lower this barrier by allowing non-experts to express goals and directly map those

objectives into low-level actions, such as movement and formation control (Liu et al., 2024; Lykov et al., 2024; Venkatesh and Min, 2025). However, this mapping remains brittle, especially in time-varying environments, because a one-time command might not account for future system changes; and multi-agent coordination amplifies small specification errors into large collective failures (Young et al., 2010; Shi and Johansson, 2013).

Large language models (LLMs) have recently improved the fidelity with which free-form text can be grounded in structured plans and codes (Huang et al., 2022; Ichter et al., 2023). However, most language-to-robot pipelines are compile-once: a prompt is translated into a plan or policy and then executed until task completion or failure (Liang et al., 2022). This open-loop usage is problematic for operation in a time-varying environment. In such settings, what matters is not only whether the initial plan is reasonable, but also whether the system can continuously incorporate new information to plan for the next action. A human-in-the-loop system offers a natural approach to solving this problem, as a human would be issuing new instructions amid changing objectives or environments. However, in a large multi-agent control system, it may be difficult for a human to pay attention to the entire system all the time. To solve this problem, we propose a mid-layer LLM supervisor as an "assistant" to the human user, which verifies that current execution matches the human's intent and repair deviations without sacrificing the stability guarantees provided by traditional control. Therefore, the human user would only need to issue a command when a major change occurs, leaving minor adjustments and adaptation to environmental changes to the LLM supervisor.

Contribution We introduce a hierarchical, human-in-the-loop control framework in which an LLM-agent supervises execution, translating

*These authors contributed equally to this work.

natural language goals to parameters for each agent, while low-level multi-agent control ensures stability and robustness. Our framework designs a centralized LLM-agent that supervises tasks proposed by a human operator and adapts execution to a changing environment, providing smooth, continuous execution without human intervention. By using an LLM supervisor, we ensure that the commands given to the drones are always aligned with the user’s intention, and by using conventional multi-agent control, we ensure that the drones faithfully adapt in a dynamic environment with minimal human intervention. In addition, we offer a theoretical guarantee that ensures convergence of the control algorithm and provides an upper bound on the controller error between LLM verifications.

2 Related Works

Classical Multi-agent Control. Multi-agent control has a long and well-established literature (Luo et al., 2010; Olfati-Saber, 2006). A common paradigm is to employ a centralized planner that generates intermediate goal representations or control inputs, which are then executed by the team (ying A. Hsieh and Kumar, 2006; Cheah et al., 2009). While central planning can be effective for coordinating complex objectives, it typically depends on a command-and-update structure and frequent communication to disseminate policies to individual agents. This reliance can become a bottleneck in real-time settings where the environment and mission objectives evolve over time. On the other hand, some studies have explored decentralized planning in which each agent’s policy relies solely on its local observations, thereby mitigating the need for real-time communication and providing robustness guarantees (Zhu et al., 2019; Zhao and Zelazo, 2016). However, those studies often overlook the importance of centralized planning and struggle to achieve complex objectives. Compared to those works, we use an LLM for central planning and periodic auto-correction, but rely on distributed multi-agent control to achieve local robust guarantees.

LLM-guided Swarm Control. Recent work has begun to use LLMs as high-level interfaces for specifying and adapting collective behaviors in robot swarms. A first line of research treats language as a convenient task specification layer and learns a low-level multi-robot policy that realizes the requested pattern or motion. For instance, Liu

et al. (2024) studies language-guided pattern formation using multi-agent reinforcement learning, where natural language prompts describe target spatial arrangements that are then achieved by decentralized robot policies. Moreover, Lykov et al. (2024) explores linguistic orchestration of UAV flocking, using an LLM to translate descriptive commands (e.g., formation type and motion style) into flock-level control objectives. Going beyond a single centralized LLM, Strobel et al. (2024) propose *LLM2Swarm*, in which LLM components support responsive reasoning, planning, and collaboration for swarms, highlighting the potential of multi-agent LLM architectures to mediate coordination. Zero-shot approaches have also emerged: Venkatesh and Min (2025) demonstrates context-aware pattern formation from high-level user intent without task-specific fine-tuning, including setups where formations may be specified via richer modalities. Despite rapid progress, most existing language-to-swarm pipelines remain largely “compile-once” at the high level: a language module produces a formation/plan, which is then executed with limited formal linkage between language-level edits and closed-loop stability. This gap is particularly acute in dynamic multi-target scenarios, where ambiguous instructions, drifting execution, or transient disturbances can cause cascading coordination errors. Our work is positioned to address this gap by coupling language-in-the-loop supervision (periodic intent verification and constrained goal edits) with a robust distributed controller that provides explicit stability/robustness guarantees between LLM updates.

3 Algorithm Design

We propose the framework UAVGENT, a three-layer hierarchy that couples (i) natural-language commands, (ii) LLM-based runtime verification/correction, and (iii) a distributed inner-loop controller with robustness guarantees. The layers operate on separated time scales: the user issues sporadic commands (outer layer), the LLM performs K periodic supervision at times $\{t_k\}_{k \in \{0, \dots, K-1\}}$ with $t_k - t_{k-1} =: \Delta_t$ for all $k \in \{1, \dots, K-1\}$ (middle layer), and the multi-agent controller runs continuously (inner layer).

In the environment, a human user commands N_a drones in \mathbb{R}^d to achieve objectives that may involve N_b independent moving targets (e.g., “Follow the red car”).

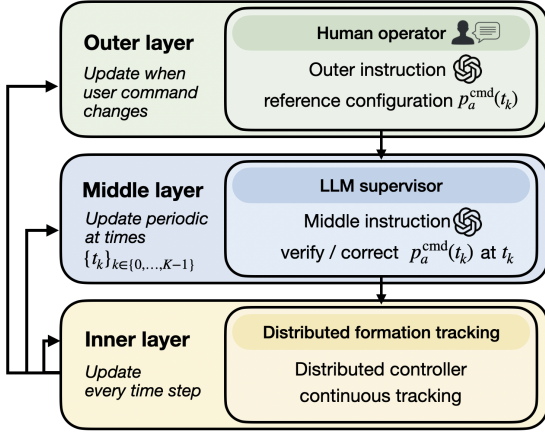


Figure 1: UAVGENT hierarchical structure

Notation. Let $p_a(t) \in \mathbb{R}^{dN_a}$ denote the stacked *drone* positions and $p_b(t) \in \mathbb{R}^{dN_b}$ denote the stacked *target* positions. Let

$$p(t) := \begin{bmatrix} p_a(t) \\ p_b(t) \end{bmatrix} \in \mathbb{R}^{dN}, \quad N := N_a + N_b.$$

We use t_k^- and t_k^+ to denote the instants immediately before and after a supervision time t_k .

Radius-induced interaction graph. The neighbor graph is induced purely by geometry: a drone considers another drone/target to be a neighbor if and only if it lies within the observation radius r . Formally, define the (time-varying) edge set

$$\mathcal{E}(t) := \left\{ \{i, j\} : i \in \mathcal{V}_a, j \in (\mathcal{V}_a \cup \mathcal{V}_b), j \neq i, \|p_i(t) - p_j(t)\| \leq r \right\},$$

i.e., edges are exactly those pairs within range of some drone sensor. Edges can disappear when nodes separate and can reappear when nodes move back within range. The LLM never outputs edges and never enforces connectivity.

3.1 Outer layer: user instruction via LLM

At any supervision instants (a subset of $\{t_k\}$), the user provides a natural-language instruction (e.g., formation type/scale, anchor choice, which target(s) to track). The LLM translates the instruction into:

1. a *nominal* drone reference configuration

$$p_a^{\text{cmd}}(t_k) \in \mathbb{R}^{dN_a}, \quad (1)$$

2. an intent summary cmd stored in memory, including a *reference type*

$$\rho \in \{\text{stationary, track, search}\}.$$

In stationary reference type, the intent is specified in the world frame (fixed anchors/coordinates). In track reference type, the intent is specified relative to one or more targets. In search reference type, the intent is at first specified in the world frame within a certain range defined by the user. When any drone finds the target, they are within the observation radius of each other, the search is completed, and all drones form a concentrated formation around the target.

3.2 Middle layer: LLM supervision

At *every* time t_k , the LLM supervisor receives (i) the latest intent cmd with reference type ρ , and (ii) the state $p(t_k^-)$. It performs auto-verification:

1. If execution is consistent with cmd, it produces no additional input.
2. If inconsistencies are detected, it outputs an updated *enforced* drone reference

$$p_a^r(t_k^+) = V(\text{cmd}, p(t_k^-)), \quad (2)$$

where $V(\cdot)$ is the LLM verification/correction operator.

Reference interpolation. On each interval $[t_k, t_{k+1}]$, $p_a^r(t)$ is held constant or smoothly interpolated. We assume p_a^r is piecewise C^1 on each such interval and may jump at t_k .

Tracking re-grounding for moving targets. If $\rho = \text{track}$, the outer layer stores a target-referenced intent rather than a fixed world-frame coordinate. In target-referenced intent, if the intent can no longer be fulfilled due to target movement (e.g. tracking a group of target starting to diverge), the system re-grounds the target-referenced intent using the current target estimate (e.g., via identity association and nearest-target heuristics with cooldown). At each check time t_k , the LLM verification (2) further updates $p_a^r(t_k^+)$ if needed in accordance with the user intent. This prevents stale coordinates from being reissued when targets move between checks.

Range-limited target search. When $\rho = \text{search}$, the outer layer maintains a description of the sought target together with a bounded region in which the target is expected to lie within. The LLM supervisor then assigns each drone a search waypoint within this region. After a drone arrives at its assigned waypoint, it performs a local scan within its sensing (observation) radius; if no detection is reported, the supervisor reassigns a new waypoint and the process repeats. If a detection occurs, the supervisor broadcasts the estimated target location, directs all drones to rendezvous at the target, and transitions the swarm to the user-specified formation.

3.3 Inner layer: distributed formation tracking on a radius-induced graph

Drones obey disturbed single-integrator dynamics

$$\dot{p}_a(t) = u_a(t) + d_a(t), \quad (3)$$

while targets evolve exogenously

$$\dot{p}_b(t) = v_b(t), \quad (4)$$

where $d_a(t)$ is an additive disturbance and $v_b(t)$ is an unknown target velocity.

At time t , each drone i uses the instantaneous neighbor set

$$\mathcal{N}_i(t) := \{j : \{i, j\} \in \mathcal{E}(t)\}.$$

The inner loop applies the distributed edge-error feedback

$$u_i(t) = \sum_{j \in \mathcal{N}_i(t)} \left((p_j(t) - p_i(t)) - (p_j^r(t) - p_i^r(t)) \right), \quad (5)$$

where $p_i^r(t)$ is the enforced drone reference for drone i , and for any target $j \in \mathcal{V}_b$ we set $p_j^r(t) := p_j(t)$ as targets are not commanded. Thus, target neighbors act as moving anchors, while drone neighbors enforce relative formation constraints.

4 Preliminaries

This section fixes graph/coordinate notation and derives the closed-loop edge-error dynamics used in Section 5. The key modeling changes are: (i) the neighbor graph is induced by the observation radius r , and (ii) targets are not actuated.

4.1 Radius-induced graph and incidence matrices

Let $\mathcal{V} = \mathcal{V}_a \cup \mathcal{V}_b$ be the node set (drones and targets), $|\mathcal{V}_a| = N_a$, $|\mathcal{V}_b| = N_b$. At time t , define the undirected neighbor graph

$$G(t) := (\mathcal{V}, \mathcal{E}(t)),$$

$$\mathcal{E}(t) := \left\{ \{i, j\} : i \in \mathcal{V}_a, j \in (\mathcal{V}_a \cup \mathcal{V}_b), j \neq i, \|p_i(t) - p_j(t)\| \leq r \right\}.$$

Choose an arbitrary orientation of the edges at each time and let $E(t) \in \mathbb{R}^{N \times m(t)}$ denote the oriented incidence matrix, with $m(t) := |\mathcal{E}(t)|$. For analytical purposes, between two supervision instances, we assume the edge set is constant on $[t_k, t_{k+1})$ and write

$$E_k := E(t) \text{ for } t \in [t_k, t_{k+1}), \quad m_k := m(t).$$

If the induced graph is disconnected, the analysis below applies on each connected component.

Define the node Laplacian on $[t_k, t_{k+1})$ as

$$L_{n,k} := E_k E_k^\top. \quad (6)$$

Let the drone-selection matrix $R_a := [I_{N_a} \ 0] \in \mathbb{R}^{N_a \times N}$ and

$$S_a := \text{diag}(\underbrace{1, \dots, 1}_{N_a}, \underbrace{0, \dots, 0}_{N_b}) = R_a^\top R_a,$$

and define the *drone-row* incidence matrix

$$E_{a,k} := R_a E_k \in \mathbb{R}^{N_a \times m_k}.$$

Similarly, let the target-selection matrix $R_b := [0 \ I_{N_b}] \in \mathbb{R}^{N_b \times N}$ and define the *target-row* incidence matrix

$$E_{b,k} := R_b E_k \in \mathbb{R}^{N_b \times m_k}.$$

4.2 Edge coordinates and error

Stack positions as $p(t) = [p_1(t)^\top \cdots p_N(t)^\top]^\top \in \mathbb{R}^{dN}$. Define the stacked edge-relative vector on $[t_k, t_{k+1})$ as

$$z(t) := (E_k^\top \otimes I_d) p(t) \in \mathbb{R}^{dm_k}. \quad (7)$$

The enforced reference is defined for drones only; targets are not commanded. Accordingly, define the node reference

$$p^r(t) := \begin{bmatrix} p_a^r(t) \\ p_b^r(t) \end{bmatrix},$$

and the induced edge-relative reference

$$z^r(t) := (E_k^\top \otimes I_d) p^r(t). \quad (8)$$

Define the edge-formation error

$$e(t) := z^r(t) - z(t). \quad (9)$$

Because $p_b^r(t) = p_b(t)$, the target components cancel and $e(t)$ depends only on drone position error:

$$e(t) = (E_{a,k}^\top \otimes I_d) (p_a^r(t) - p_a(t)) \in \text{range}(E_{a,k}^\top \otimes I_d). \quad (10)$$

4.3 Closed-loop edge-error dynamics

Let drone and target dynamics be (3)–(4) and define the stacked exogenous input

$$d(t) := \begin{bmatrix} d_a(t) \\ v_b(t) \end{bmatrix}.$$

The distributed control law (5) can be written in stacked form on $[t_k, t_{k+1})$ as

$$u_a(t) = (E_{a,k} \otimes I_d) e(t), \quad (11)$$

i.e., the node control is computed from incident edge errors and applied only to drones.

On any interval where p_a^r is C^1 , differentiating (9) and using the dynamics yields

$$\dot{e}(t) = -(L_{e,k}^a \otimes I_d) e(t) + w(t), \quad (12)$$

where the *actuated edge Laplacian* is

$$L_{e,k}^a := E_{a,k}^\top E_{a,k} = E_k^\top S_a E_k \succeq 0, \quad (13)$$

and the additive input is

$$w(t) := \dot{z}^r(t) - (E_k^\top \otimes I_d) d(t). \quad (14)$$

Using $p^r = [p_a^r; p_b]$ and $d = [d_a; v_b]$, the v_b terms cancel inside (14), giving the equivalent expression

$$w(t) = (E_{a,k}^\top \otimes I_d) (p_a^r(t) - d_a(t)) \in \text{range}(E_{a,k}^\top \otimes I_d). \quad (15)$$

Jumps at supervision times. At t_k , $p(t)$ is continuous but p_a^r may jump. If the neighbor graph does not change at t_k , then $e(t_k^+) = e(t_k^-) + \Delta z_k^r$ with $\Delta z_k^r := z^r(t_k^+) - z^r(t_k^-)$. If the neighbor graph changes due to the radius rule, then E_k changes and $e(t_k^+)$ is reinitialized.

5 Theoretical Guarantee

In this section, we prove the robustness within an arbitrary interval $[t_k, t_{k+1})$. We first introduce a few assumptions for the derivation of a theoretical guarantee. We point out that those assumptions are for the convenience of analysis and are not strictly required by the algorithm, as shown in Section 6.

Assumption 1. *On some fixed $[t_k, t_{k+1})$,*

- (A1) *E_k is constant, and the enforced edge-relative reference is held constant, i.e. $\dot{z}^r(t) = 0$.*
- (A2) *the target motion is formation-feasible in the sense that (16) admits at least one solution $\dot{p}_a^r(\cdot)$ on $[t_k, t_{k+1})$, and that the reference generator selects a feasible solution with bounded speed $\|\dot{p}_a^r(t)\| \leq \bar{v}_r$ for some $\bar{v}_r < \infty$.*
- (A3) *The drone disturbance and target velocity are bounded as $\|d_a(t)\| \leq \bar{d}_a$, $\|v_b(t)\| \leq \bar{v}_b$.*

We note that since $z^r(t) = (E_k^\top \otimes I_d)p^r(t)$ with $p^r(t) = [p_a^r(t); p_b(t)]$, Assumption 1 (A1) is equivalent to the *compatibility condition*

$$\begin{aligned} 0 = \dot{z}^r(t) &= (E_k^\top \otimes I_d) \begin{bmatrix} \dot{p}_a^r(t) \\ v_b(t) \end{bmatrix} \\ &= (E_{a,k}^\top \otimes I_d) \dot{p}_a^r(t) + (E_{b,k}^\top \otimes I_d) v_b(t). \end{aligned} \quad (16)$$

Moreover, given Assumption 1, we have that the stacked exogenous input $d(t) = [d_a(t); v_b(t)]$ satisfies

$$\|d(t)\| \leq \bar{d} := \bar{d}_a + \bar{v}_b,$$

and the node-level effective input satisfies

$$\|\dot{p}_a^r(t) - d_a(t)\| \leq \bar{v} := \bar{v}_r + \bar{d}_a.$$

In most time intervals, the above assumption is natural: when drones maintain their formations, their relative positions should remain relatively constant, so their neighbor relations do not change either. The above assumption would be broken if the movement of targets renders the formation impossible to maintain. As we show in Section 6.1, the proposed algorithm still handles the scenario with ease. Moreover, as the disturbances in real-world scenarios are usually caused by wind or current, which can be assumed to be upper bounded. For both stationary and tracking tasks, when formation is required, the reference edge-relative positions of the drones should stay constant.

Theorem 1 (Exponential ISS of edge-formation error). *Fix k and consider an interval $[t_k, t_{k+1}]$ where Assumption 1 holds. Further assume the corresponding graph is connected (or restrict to a connected component). Let $e(t)$ satisfy the closed-loop edge-error dynamics (12) with additive input $w(t)$ given by (14).*

Let $\lambda_k > 0$ denote its smallest strictly positive eigenvalue of the edge Laplacian:

$$\lambda_k := \lambda_{\min}^+(L_{e,k}^a) = \lambda_{\min}^+(E_{a,k} E_{a,k}^\top). \quad (17)$$

Then, for any $t \in [t_k, t_{k+1}]$,

$$\|e(t)\| \leq e^{-\lambda_k(t-t_k)} \|e(t_k^+)\| + \int_{t_k}^t e^{-\lambda_k(t-s)} \|w(s)\| ds. \quad (18)$$

In particular, if $\|w(t)\| \leq \bar{w}$ on $[t_k, t_{k+1}]$ then

$$\|e(t)\| \leq e^{-\lambda_k(t-t_k)} \|e(t_k^+)\| + \frac{\bar{w}}{\lambda_k} (1 - e^{-\lambda_k(t-t_k)}). \quad (19)$$

The proof of Theorem 1 is deferred to Section C. We point out that at an LLM supervision instant t_k , if the neighbor graph does not change (so E_k is unchanged across t_k) and z^r jumps by $\Delta z_k^r := z^r(t_k^+) - z^r(t_k^-)$, then

$$\begin{aligned} e(t_k^+) &= e(t_k^-) + \Delta z_k^r, \\ \|e(t_k^+)\| &\leq \|e(t_k^-)\| + \|\Delta z_k^r\|. \end{aligned} \quad (20)$$

If instead the radius-induced graph changes at t_k , then $e(t_k^+)$ is reinitialized in the new edge coordinates as stated in Section 4.3 and serves as the initial condition for (18) on the next interval.

5.1 Checking-period guideline

Define the drone reference-tracking error

$$\tilde{p}_a(t) := p_a^r(t) - p_a(t) \in \mathbb{R}^{dN_a}, \quad t \in [t_k, t_{k+1}].$$

Using the drone dynamics (3), the stacked controller (11), and the identity $e(t) = (E_{a,k}^\top \otimes I_d) \tilde{p}_a(t)$ from (10), we obtain

$$\begin{aligned} \dot{\tilde{p}}_a(t) &= \dot{p}_a^r(t) - \dot{p}_a(t) = \dot{p}_a^r(t) - u_a(t) - d_a(t) \\ &= -(E_{a,k} \otimes I_d) e(t) + (\dot{p}_a^r(t) - d_a(t)) \\ &= -(E_{a,k} E_{a,k}^\top \otimes I_d) \tilde{p}_a(t) + \nu(t), \end{aligned}$$

where $\nu(t) := \dot{p}_a^r(t) - d_a(t)$.

If the connected component under consideration contains at least one target (equivalently, the restriction is *anchored* so that $E_{a,k} E_{a,k}^\top \succ 0$ on that

component), then the semigroup $e^{-(E_{a,k} E_{a,k}^\top \otimes I_d)t}$ contracts at rate at least λ_k on \mathbb{R}^{dN_a} . Applying variation-of-constants to (21) yields, for any $t \in [t_k, t_{k+1}]$,

$$\|\tilde{p}_a(t)\| \leq e^{-\lambda_k(t-t_k)} \|\tilde{p}_a(t_k^+)\| + \int_{t_k}^t e^{-\lambda_k(t-s)} \|\nu(s)\| ds. \quad (21)$$

In particular, if $\|\nu(t)\| \leq \bar{\nu}$ on $[t_k, t_{k+1}]$, then

$$\|\tilde{p}_a(t)\| \leq e^{-\lambda_k(t-t_k)} \|\tilde{p}_a(t_k^+)\| + \frac{\bar{\nu}}{\lambda_k} (1 - e^{-\lambda_k(t-t_k)}), \quad (22)$$

Corollary 1 (LLM relative accuracy for edge-level tolerance). *Consider interval $[t_k, t_{k+1}]$ satisfying Assumption 1. Denote $\bar{w} := \|E_k^\top \otimes I_d\| \bar{d}$ so that $\|w(t)\| \leq \bar{w}$. Further assume that the LLM grounding error in edge coordinates is uniformly bounded by $\varepsilon_z \geq 0$:*

$$\sup_{t \in [t_k, t_{k+1}]} \|z^r(t) - z^*(t)\| \leq \varepsilon_z.$$

Fix a desired edge tolerance $\delta_z > 0$ at time t_{k+1}^- : $\|z(t_{k+1}^-) - z^(t_{k+1}^-)\| \leq \delta_z$. If*

$$\eta_{\max}^{(z)}(\delta_z, \Delta_t, \varepsilon_z) := e^{\lambda_k \Delta_t} (\delta_z - \varepsilon_z) - \frac{\bar{w}}{\lambda_k} (e^{\lambda_k \Delta_t} - 1) \geq 0,$$

and the post-check edge error satisfies $\|e(t_k^+)\| \leq \eta_{\max}^{(z)}(\delta_z, \Delta_t, \varepsilon_z)$, then $\|z(t_{k+1}^-) - z^(t_{k+1}^-)\| \leq \delta_z$.*

Remark 1 (Feasibility and interpretation). *The threshold $\eta_k^{\max}(\delta_z, \Delta_t, \varepsilon_z)$ can be negative if δ is too small relative to (i) the LLM grounding error ε_z , (ii) the effective input level \bar{w} , and (iii) the check interval Δ_t . In particular, even if the controller could instantaneously enforce $\tilde{p}_a(t_k^+) = 0$, the bound (22) implies the unavoidable contribution $\frac{\bar{w}}{\lambda_k} (1 - e^{-\lambda_k \Delta_t})$, so a necessary condition for feasibility is*

$$\varepsilon_z + \frac{\bar{w}}{\lambda_k} (1 - e^{-\lambda_k \Delta_t}) \leq \delta_z.$$

The above results extend to a longer time horizon as long as the user intent stays consistent. We defer the detailed theorem and discussions to Section D.

6 Simulation

In this section, we evaluate the proposed framework in two representative case studies. The results demonstrate how high-level natural-language commands are translated into coordinated multi-drone behaviors, and how LLM-based supervision enables robust adaptation to dynamic environments, as detailed below.

6.1 Police-chasing scenario

We simulate 3 police-assisted pursuit scenarios, each with a different map, user command, number of drones, or configuration of suspect cars. The scenarios are represented in a three-dimensional environment ($d = 3$), where a human operator issues high-level natural-language commands and the proposed three-layer architecture coordinates a team of drones to track three suspect vehicles (targets). Drone positions satisfy $p_i(t) \in \mathbb{R}^3$ and are initialized randomly, as in Figure 2a; the suspect cars evolve on the ground plane, while drones maintain a commanded operating altitude band.

Phase I: convoy tracking in grid formation. Initially, the officer commands the swarm to *follow the group of cars in a [grid] formation*. The system instantiates the specified formation (grid) and tracks the suspects as a convoy while the cars remain sufficiently close, see Figure 2b.

Phase II: suspects split and local reassignment. After the suspects detect surveillance, the three cars split and move in different directions. Once the inter-target separation exceeds a preset threshold, the inner layer performs a fast, local reassignment based on target-proximity, producing three pursuit sub-swarms. During this transient, the formation quality degrades: agents migrate between sub-swarms, the formation geometry (grid) is temporarily distorted, and the three groups can become imbalanced in size, as in Figure 2d and Figure 4.

Phase III: mid-layer verification and regrouping. At the subsequent verification instances, the mid-layer LLM supervisor detects distorted grids and uneven group sizes, then applies automatic correction: it re-grounds the command using the *current* target estimates, rebalances the drone-target assignments to yield roughly equal subgroup sizes, and regenerates clean per-target formation references (grid). The inner layer then recenters each subswarm to an organized grid while continuing to track the assigned car as in Figure 2e and Figure 4.

Phase IV: human formation switching for target disambiguation. Finally, the officer issues a command to visually distinguish suspects: *one group forms a [circle], one forms a [square], and one forms a [cross]*. The supervisor updates the per-target formation templates accordingly, and the inner layer drives each subgroup to its new formation while preserving target tracking, as shown in

Figure 2f and Figure 4.

Results and Discussions In the police-chasing scenarios, we focus on testing the target tracking ability of the proposed framework and how the LLM supervision helps in correcting formation-command mismatch caused by the change of system dynamics when the suspects split. We see that when the targets initially split, the inner layer distributed control helps to roughly distribute drones to each target (Figure 2b), while the mid-layer LLM auto-verification gives a relative position assignment to each drone more aligned with human-intent (Figure 2e and Figure 4). In the entire process, there is no involvement of human user giving command for adaptation to environmental changes, and the command they give demonstrates new user intentions, which are then incorporated into LLM supervision in the future. Overall, the LLM supervision performed as intended and greatly reduced the human involvement in the process.

6.2 LLM-guided search and rescue in a forest environment

We consider 3 search-and-rescue scenarios in which a single missing person is believed to be within a bounded forest region under severe environmental conditions. An officer issues high-level instructions through the LLM interface, and the drones are assigned random coordinates in the forest to search for the missing person.

Phase I: randomized waypoint assignment for area search. At the start of the mission, all drones are located at the start point, as in Figure 3a. The LLM supervisor generates candidate search waypoints within the user-specified search region. Each drone is assigned a waypoint to inspect, yielding a spatially distributed search pattern without requiring the officer to micromanage coverage.

Phase II: event-driven re-tasking upon negative observations. When a drone reaches its assigned waypoint without detecting the missing person anywhere along its path, it reports a *clear* status to the supervisor. The LLM then issues a new waypoint assignment to that drone, thereby maintaining continuous exploration of the region. This process repeats until a detection event occurs. In this phase, the swarm behavior is dominated by successive waypoint updates, while the inner-loop controller ensures stable motion between updates and smooth transitions when new waypoints are issued,

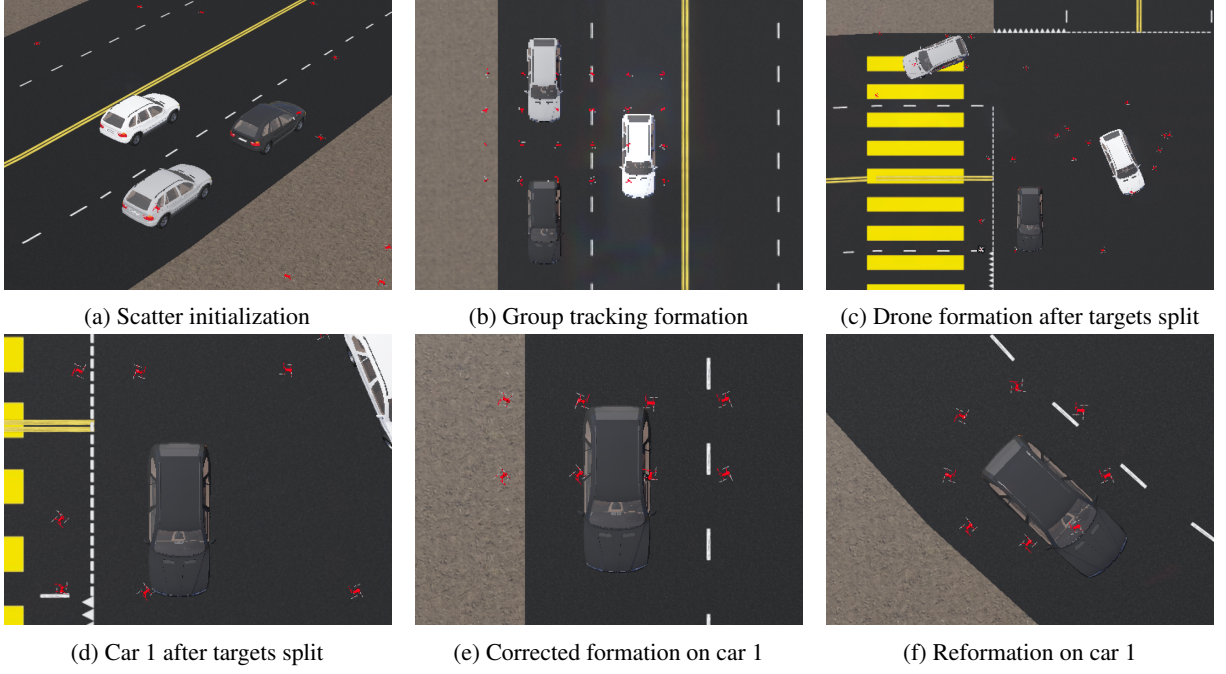


Figure 2: In Figure 2a, 24 drones are initially scattered around the target vehicles. The user commands the drones to form a grid and track the vehicles (Figure 2b). As the vehicles diverge, the inner-layer controller splits the swarm to track each target, temporarily degrading the formation (Figure 2c). The LLM supervisor then re-centers and rebalances the sub-swarms (Figure 2e). Finally, the user requests reformation into a circle, square, and cross (Figure 2f). Additional details are shown in Figure 4.

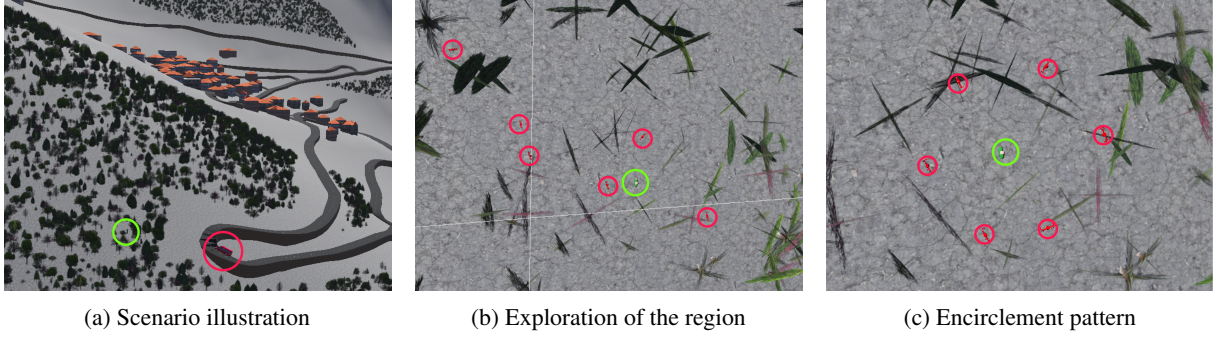


Figure 3: In Figure 3a, we show a mountain search-and-rescue scenario with a rescue vehicle (red circle) and a missing person (green circle). After the user commands the drones to explore, they move to assigned waypoints while searching the region (Figure 3b). Upon detection, the drones form an encirclement around the target (Figure 3c).

as shown in Figure 3b.

Phase III: detection-triggered rally and encirclement. If any drone detects the missing person, it immediately reports the detection and location. The LLM supervisor switches the mission objective from *search* to *assist* by directing all drones to converge to the detected target location and adopt an encirclement pattern. Specifically, the supervisor issues a circle formation reference centered at the detected position to mark the location for ground responders and maintain line-of-sight coverage. The resulting circle formation provides a persistent vi-

sual and sensing cue to guide the rescue effort, as shown in Figure 3c.

Reported outputs. We summarize this simulation by reporting (i) time-to-detection, (ii) number of waypoint reassignments prior to detection, (iii) search efficiency indicators (e.g., fraction of candidate waypoints cleared versus elapsed time), and (iv) formation quality during the encirclement phase (e.g., circle-radius error and inter-drone spacing regularity). Representative 3D snapshots illustrate the transition from randomized search to coordinated target encirclement.

7 Limitations

This work demonstrates a framework of using LLM to assist with real-life UAV distributed control. It did not use the newly developed visual-language-action model or multimodal policies, some of which have been introduced in Section 2. The authors anticipate that using those tools would further enhance the framework’s functionality and bring it one step closer to real-world deployment. Furthermore, we introduce only three human intentions, but the proposed framework is flexible enough to incorporate additional ones as the user determines necessary.

References

Chien Chern Cheah, Saing Paul Hou, and Jean Jacques E. Slotine. 2009. [Region-based shape control for a swarm of robots](#). *Automatica*, 45(10):2406–2411.

Wenlong Huang, Pieter Abbeel, Deepak Pathak, and Igor Mordatch. 2022. [Language models as zero-shot planners: Extracting actionable knowledge for embodied agents](#). In *Proceedings of the 39th International Conference on Machine Learning*, volume 162 of *Proceedings of Machine Learning Research*, pages 9118–9147. PMLR.

Brian Ichter, Anthony Brohan, Noah Brown, Yevgen Chebotar, Omar Cortes, Byron David, Chelsea Finn, Chuyuan Kelly Fu, Keerthana Gopalakrishnan, Karol Hausman, Alex Herzog, Daniel Ho, Jasmine Hsu, Julian Ibarz, Eric Jang, Dmitry Kalashnikov, Yuheng Kuang, Kuang-Huei Lee, Sergey Levine, and 21 others. 2023. [Do as i can, not as i say: Grounding language in robotic affordances](#). In *Proceedings of The 6th Conference on Robot Learning*, volume 205 of *Proceedings of Machine Learning Research*, pages 287–318. PMLR.

Jacky Liang, Wenlong Huang, Fei Xia, Peng Xu, Karol Hausman, Brian Ichter, Pete Florence, and Andy Zeng. 2022. [Code as policies: Language model programs for embodied control](#). *Preprint*, arXiv:2209.07753.

Hsu-Shen Liu, So Kuroki, Tadashi Kozuno, Wei-Fang Sun, and Chun-Yi Lee. 2024. [Language-guided pattern formation for swarm robotics with multi-agent reinforcement learning](#). In *2024 IEEE/RSJ International Conference on Intelligent Robots and Systems (IROS)*, pages 8998–9005.

Xiaoyuan Luo, Shaobao Li, and Xinping Guan. 2010. [Flocking algorithm with multi-target tracking for multi-agent systems](#). *Pattern Recognition Letters*, 31(9):800–805.

Artem Lykov, Sausar Karaf, Mikhail Martynov, Valerii Serpiva, Aleksey Fedoseev, Mikhail Konenkov, and Dzmitry Tsetserukou. 2024. [Flockgpt: Guiding uav flocking with linguistic orchestration](#). In *2024 IEEE International Symposium on Mixed and Augmented Reality Adjunct (ISMAR-Adjunct)*, pages 485–488.

R. Olfati-Saber. 2006. [Flocking for multi-agent dynamic systems: algorithms and theory](#). *IEEE Transactions on Automatic Control*, 51(3):401–420.

Jorge Peña Queralta, Jussi Taipalmaa, Bilge Can Pullinen, Victor Kathan Sarker, Tuan Nguyen Gia, Hannu Tenhunen, Moncef Gabbouj, Jenni Raitoharju, and Tomi Westerlund. 2020. [Collaborative multi-robot search and rescue: Planning, coordination, perception, and active vision](#). *IEEE Access*, 8:191617–191643.

Guodong Shi and Karl Henrik Johansson. 2013. [Multi-agent robust consensus: Convergence analysis and application](#). *SIAM Journal on Control and Optimization*. ArXiv:1108.3226 version available.

Volker Strobel, Marco Dorigo, and Mario Fritz. 2024. [Llm2swarm: Robot swarms that responsively reason, plan, and collaborate through llms](#). *Preprint*, arXiv:2410.11387.

Vishnunandan L. N. Venkatesh and Byung-Cheol Min. 2025. [Zerocap: Zero-shot multi-robot context aware pattern formation via large language models](#). *Preprint*, arXiv:2404.02318.

Mong Ying A. Hsieh and V. Kumar. 2006. [Pattern generation with multiple robots](#). In *Proceedings 2006 IEEE International Conference on Robotics and Automation, 2006. ICRA 2006.*, pages 2442–2447.

George F. Young, Luca Scardovi, and Naomi E. Leonard. 2010. Robustness of noisy consensus dynamics with directed communication. In *Proceedings of the American Control Conference*, pages 6312–6317.

Shiyu Zhao and Daniel Zelazo. 2016. [Bearing rigidity and almost global bearing-only formation stabilization](#). *IEEE Transactions on Automatic Control*, 61(5):1255–1268.

Hai Zhu, Jelle Juhl, Laura Ferranti, and Javier Alonso-Mora. 2019. [Distributed multi-robot formation splitting and merging in dynamic environments](#). In *2019 International Conference on Robotics and Automation (ICRA)*, pages 9080–9086.

A Additional Figures and Simulations

In this section, we provide some additional figures for the existing simulation, together with additional scenarios under the same general settings.

Police-chasing scenario 1. In Figure 4, we provide a detailed visualization of the drone layouts over the target vehicles throughout the scenario. The suspect vehicles initially travel together along the road and then diverge in different directions at the intersection. The drone layouts are automatically updated by the mid-layer LLM supervisor in response to these changes. After the operator issues additional commands for the drones to adopt different formations (circle, square, and cross), the outer layer processes the new instructions and the middle layer reformulates the corresponding formation references accordingly. The inner layer continues to operate at each time step to ensure that the desired formation is achieved.

Police-chasing scenario 2. In Figure 5, the operator issues a command as *"Three suspects are attempting to escape. Form a circle like a coordinated police dragnet and track all three targets."* The suspect vehicles initially travel together along the road and then diverge in different directions at the intersection. As the targets separate, the system automatically adapts the swarm configuration to maintain coordinated tracking of all three vehicles. Compared to grid-based convoy tracking, enforcing a circular encirclement with a larger swarm (24 drones in this example) introduces additional geometric and assignment complexity. Nevertheless, the proposed architecture handles this case in the same unified manner by grounding the user instruction into formation references, dynamically reassigning drones to targets, and continuously updating the control inputs through the inner layer. After the drones form three encirclement groups around the three vehicles, the operator updates the instruction *"Stop tracking all the targets."*. The outer and middle layers process this new command, update the swarm configuration, and deactivate the tracking objective. This scenario demonstrates that the proposed framework can robustly handle both the splitting and reconvergence of targets, enabling the swarm to dynamically merge and reform joint behaviors as the task structure evolves.

Police-chasing scenario 3. In Figure 6, the operator issues a command such as *"Three suspects are attempting to escape. Form a circle like a coordinated police dragnet and track all three targets."*

The suspect vehicles initially travel together along the road and then diverge in different directions at the intersection. As the targets separate, the system automatically adapts the swarm configuration to maintain coordinated tracking of all three vehicles. At a later time, the vehicles execute U-turns, reverse direction, and return toward the intersection, where they eventually merge again onto a common path. The 24 drones subsequently regroup, and under the LLM supervision of the mid-layer, re-form a single encirclement above the three vehicles.

Search-and-rescue scenario 1. This scenario has been introduced and discussed in Section 6.2 with Figure 3.

Search-and-rescue scenario 2. This scenario follows the same procedure as Scenario 1 (see Section 6.2), but places the target at a different location in the environment (see Figure 7). Figure 7a shows the initial deployment of the drones, while Figure 7b illustrates the ongoing search process with distributed location exploration. Upon detection, the drones transition to a three-dimensional cube formation centered at the target, providing volumetric coverage and better visibility, as shown in Figure 7c.

Search-and-rescue scenario 3. This scenario follows the same overall procedure, but incorporates automatic correction by the LLM supervisor and considers an enlarged search region (see Figure 8). Figure 8a shows the initial deployment of the drones, while Figure 8b illustrates the search process within the initial search area. As the search region is expanded through automatic correction, the drones adapt their exploration accordingly, as shown in Figure 8c.

B Prompts for Users and LLM-supervisor

This section summarizes the prompts used in the scenarios described above.

Motion Descriptor
You are an instruction parser for a multi-agent control system. Rules: 1. "mode": - "track" if the user mentions tracking, following, escorting, or maintaining formation around moving targets. - "search" if the user mentions searching,

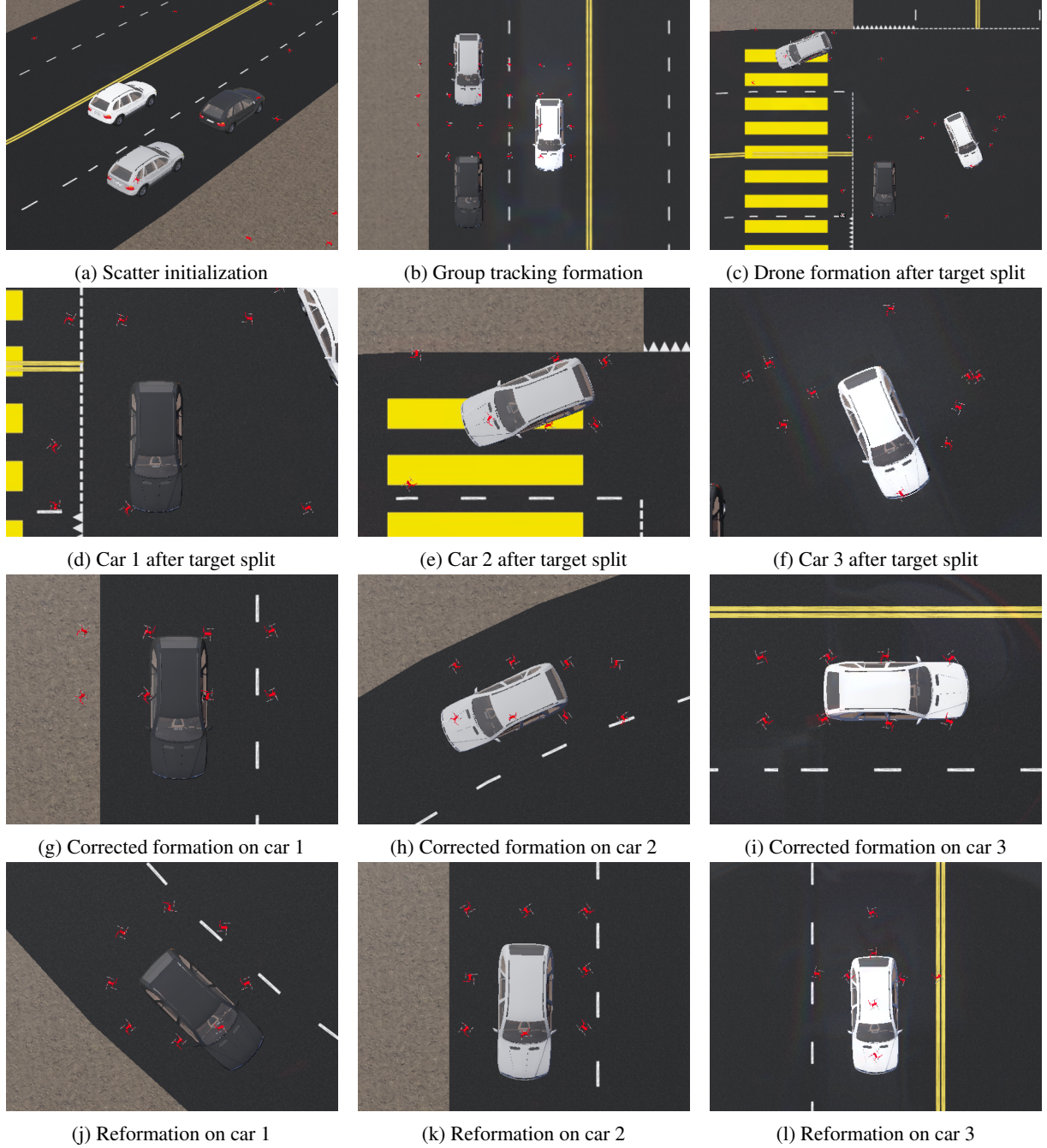


Figure 4: In Figure 4a, we have 24 drones scattered around the target cars. The user then commands the drones to form a grid around the cars with LLM, as shown in Figure 4b. As the cars move toward the road intersection, they diverge in different directions. The inner-layer control algorithm has the group of drones diverted to track different cars, as shown in Figure 4c. However, the low-level control heuristic does not ensure the drones maintain the formation exactly during splitting. Lastly, the LLM auto-verification recenters each drone on the target and rebalances the group for each target, as shown in Figure 4g, Figure 4h, and Figure 4i. The user then issues additional commands to reform the groups into a circle, square, and cross, as shown in Figure 4j, Figure 4k, and Figure 4l.

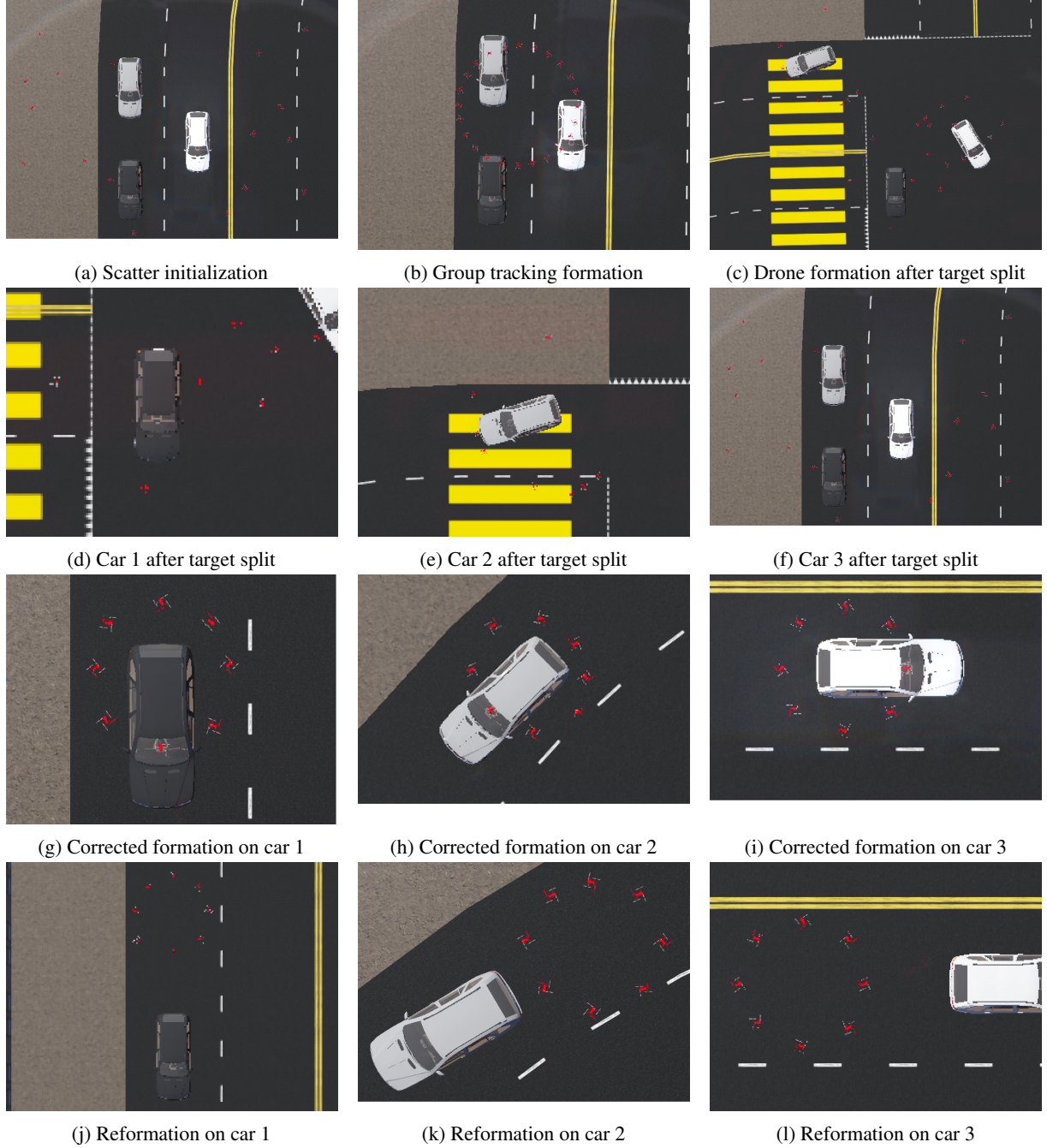
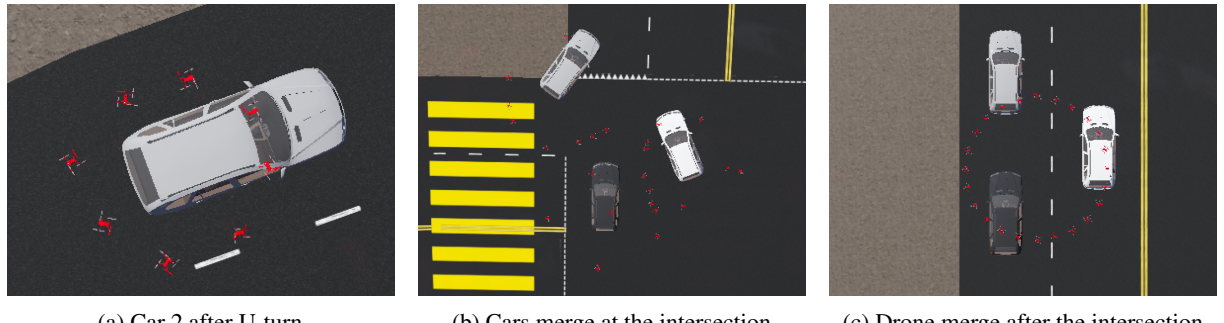
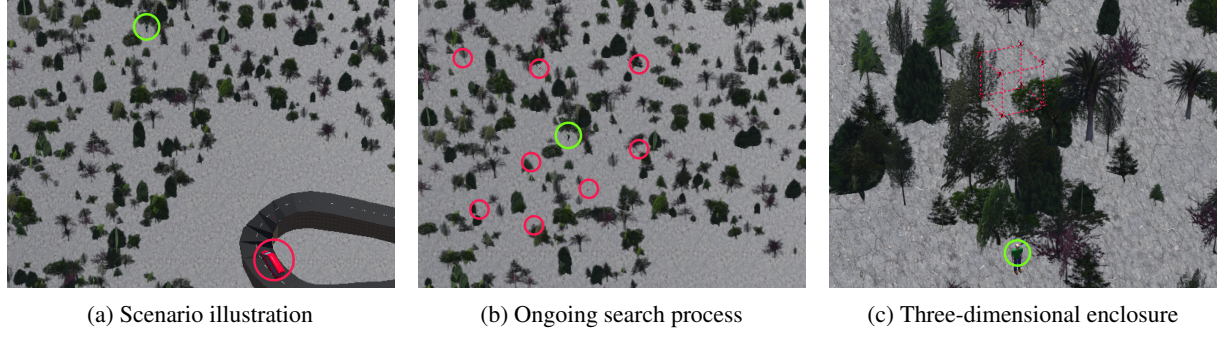


Figure 5: In Figure 5a, we have 24 drones scattered around the target cars. The user then commands the drones to form a circle around the cars with LLM, as shown in Figure 5b. As the cars move toward the road intersection, they diverge to different directions. The inner-layer control algorithm has the group of drones diverted to track different cars, as shown in Figure 5c. However, the low-level control heuristic does not organize the car to maintain the formation exactly during the splitting process. Lastly, the LLM auto-verification recenters each drone on the target and rebalances the group for each target, as shown in Figure 5d, Figure 5e, and Figure 5f. The user then issues additional commands to not tracking, as shown in Figure 5j, Figure 5k, and Figure 5l.



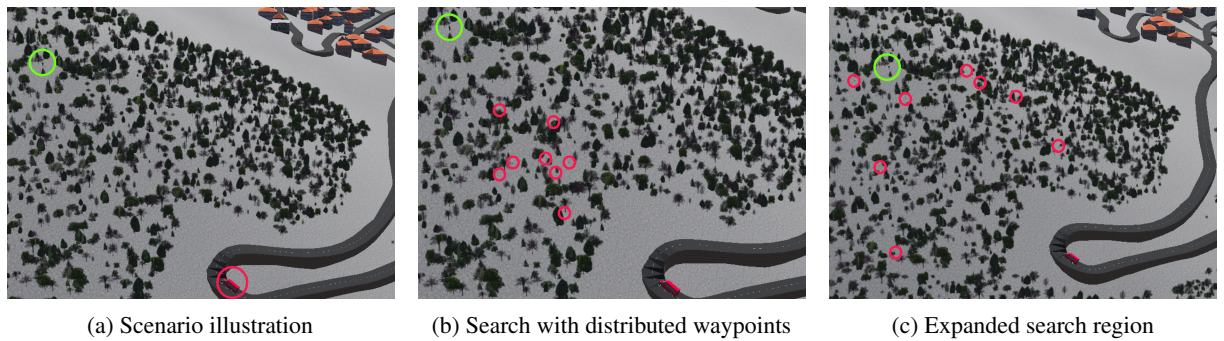
(a) Car 2 after U-turn (b) Cars merge at the intersection (c) Drone merge after the intersection

Figure 6: In Figure 6a, the drones maintain a circular formation while vehicle 2 executes a U-turn. In Figure 6b, all vehicles reconverge at the intersection. In Figure 6c, the vehicles merge onto a common path, and the drones correspondingly regroup into a single encirclement.



(a) Scenario illustration (b) Ongoing search process (c) Three-dimensional enclosure

Figure 7: Search-and-rescue Scenario 2 with the target located at a different position. In this scenario, eight drones are deployed. (a) Initial deployment of the rescue vehicle and the target. (b) Ongoing search process with distributed waypoint exploration. (c) Upon detection, the drones form a three-dimensional cube formation around the target, providing volumetric coverage.



(a) Scenario illustration (b) Search with distributed waypoints (c) Expanded search region

Figure 8: Search-and-rescue Scenario 3 with the target located at a farther distance. In this scenario, eight drones are deployed. (a) Initial deployment of the rescue vehicle and the target. (b) Ongoing search process with distributed waypoint exploration within the initial search region. (c) Search region expansion through automatic correction, with the drones adapting their exploration accordingly.

scanning, exploring, or patrolling.

- "stationary" otherwise.
- 2. "tracking":
- true if mode is "track".
- false otherwise.
- 3. Each "group" corresponds to one target mentioned by the user (e.g. car1, car2).
- 4. "formation":
- Use the shape mentioned by the user.
- Use "grid" if not specified.
- 5. "even_split":
- true only if the user explicitly says "evenly", "equally", or "balanced".
- false otherwise.
- 6. "spacing":
- Use the number if provided.
- Default to 2 if not specified.

Output JSON only. No extra text.

1,x1,y1,z1
...
Only output the table.

Auto-correction

You are a multi-agent formation checker.
Goal: Decide if the current drone formation meets the user's intent or if it should be revised.

INPUT:

- 1) USER INSTRUCTION: USER_TEXT

- Describes desired formation/behavior.
- 2) CURRENT FORMATION (CSV): FEEDBACK_CSV
- One or multiple groups.
- Groups separated by lines starting with "# group" or "—".
- Coordinates are 3D relative positions: id,x,y,z

CHECK: Compare the user instruction with the current coordinates. Consider:

- Formation shape (grid, circle, line, cluster)
- Group separation (if multiple targets implied)
- Rough symmetry/alignment

Small numeric deviations should NOT trigger revision.

OUTPUT (STRICT JSON ONLY):

```
{
  "feedback": true/false,
  "reason": "Short explanation (1-2 sentences)"
}
```

Examples:

```
"feedback": false, "reason": "Grid matches user request."
"feedback": true, "reason": "One cluster but multiple groups requested."
```

Formation Instruction

You are a formation geometry generator.
Your task is to output 3D formation offsets (x,y,z) for N drones, relative to the formation center at (0,0) and at a height offset z above the ground.

Input:

- Formation shape (e.g., circle, square, grid, cross, spiral).
- Number of drones N.
- Optional spacing (meters), default is 1.0 meter.
- Optional height offset z (meters above ground), default is 0.

Rules:

- Output exactly N points.
- Points are relative offsets from the formation center (0,0).
- z represents the vertical offset above the ground.
- Use simple geometry consistent with the requested shape.
- If spacing is given, neighboring drones should be approximately spacing meters apart.
- Do not place multiple drones at the same location.

Output format (CSV only, no extra text):

id,x,y,z
0,x0,y0,z0

C Proof of Theorem 1 and Corollary 1

In this section, we offer the proof of Theorem 1 and Corollary 1.

Proof of Theorem 1.

Step 1: Closed-loop error dynamics with exogenous targets. On $[t_k, t_{k+1})$, the incidence matrix E_k is constant. Differentiate the edge-error definition (9):

$$\dot{e}(t) = \dot{z}^r(t) - (E_k^\top \otimes I_d)\dot{p}(t).$$

Using the stacked dynamics from Section 3.3, namely $\dot{p}_a = u_a + d_a$ and $\dot{p}_b = v_b$, and the stacked neighbor-feedback controller (11) (i.e., $u_a = (E_{a,k} \otimes I_d)e$), we obtain

$$\begin{aligned} \dot{e}(t) &= \dot{z}^r(t) - (E_k^\top \otimes I_d) \begin{bmatrix} \dot{p}_a(t) \\ \dot{p}_b(t) \end{bmatrix} \\ &= \dot{z}^r(t) - (E_k^\top \otimes I_d) \begin{bmatrix} (E_{a,k} \otimes I_d)e(t) + d_a(t) \\ v_b(t) \end{bmatrix} \\ &= \dot{z}^r(t) - (E_k^\top S_a E_k \otimes I_d)e(t) - (E_k^\top \otimes I_d) \begin{bmatrix} d_a(t) \\ v_b(t) \end{bmatrix}. \end{aligned}$$

To emphasize how exogenous target motion enters, note that by construction $z^r(t) = (E_k^\top \otimes I_d)p^r(t)$ with $p^r(t) = [p_a^r(t); p_b^r(t)]$, hence

$$\dot{z}^r(t) = (E_k^\top \otimes I_d) \begin{bmatrix} \dot{p}_a^r(t) \\ v_b(t) \end{bmatrix}.$$

Substituting into $w(t)$ cancels the target-velocity term $v_b(t)$, yielding the simplified input expression (15):

$$w(t) = (E_{a,k}^\top \otimes I_d)(\dot{p}_a^r(t) - d_a(t)).$$

Under Assumption 1(A1), $\dot{z}^r(t) = 0$ on $[t_k, t_{k+1})$, so (16) holds and

$$w(t) = \dot{z}^r(t) - (E_k^\top \otimes I_d)d(t) = -(E_k^\top \otimes I_d)d(t).$$

By (16), this is equivalent to the simplified expression above, and in particular $w(t) \in \text{range}(E_{a,k}^\top \otimes I_d)$.

Thus, targets affect the error dynamics only through how the enforced drone reference p_a^r evolves.

Step 2: Invariance of the admissible subspace. From (10), we have $e(t) \in \text{range}(E_{a,k}^\top \otimes I_d)$ for all $t \in [t_k, t_{k+1})$. From (15), we also have $w(t) \in \text{range}(E_{a,k}^\top \otimes I_d)$ for all t . Therefore, the dynamics (12) evolve on the invariant subspace $\text{range}(E_{a,k}^\top \otimes I_d)$.

Step 3: Strict positivity of $L_{e,k}^a$ on $\text{range}(E_{a,k}^\top)$. The matrix $L_{e,k}^a = E_{a,k}^\top E_{a,k}$ is symmetric positive semidefinite, with

$$\ker(L_{e,k}^a) = \ker(E_{a,k}).$$

Moreover, for any matrix M , $\text{range}(M^\top) = (\ker(M))^\perp$. Applying this with $M = E_{a,k}$ gives

$$\text{range}(E_{a,k}^\top) = (\ker(E_{a,k}))^\perp = (\ker(L_{e,k}^a))^\perp.$$

Hence, the restriction of $L_{e,k}^a$ to $\text{range}(E_{a,k}^\top)$ is positive definite.

Let the eigenvalues of $L_{e,k}^a$ be

$$0 = \mu_1 = \dots = \mu_q < \mu_{q+1} \leq \dots \leq \mu_{m_k},$$

where $q = \dim \ker(L_{e,k}^a)$. Then, by definition, the smallest strictly positive eigenvalue is $\mu_{q+1} = \lambda_{\min}^+(L_{e,k}^a) =: \lambda_k$. Consequently, for all $\xi \in \text{range}(E_{a,k}^\top)$,

$$\xi^\top L_{e,k}^a \xi \geq \lambda_k \|\xi\|^2. \quad (23)$$

Finally, since $E_{a,k}^\top E_{a,k}$ and $E_{a,k} E_{a,k}^\top$ share identical nonzero eigenvalues (squares of the nonzero singular values of $E_{a,k}$), (17) holds.

Step 4: Semigroup contraction and variation-of-constants. Because $L_{e,k}^a \otimes I_d$ is symmetric, it is diagonalizable with nonnegative real eigenvalues. On the invariant subspace $\text{range}(E_{a,k}^\top \otimes I_d)$, the Rayleigh bound (23) implies that the semigroup $e^{-(L_{e,k}^a \otimes I_d)t}$ contracts at rate at least λ_k :

$$\|e^{-(L_{e,k}^a \otimes I_d)t} x\| \leq e^{-\lambda_k t} \|x\|, \quad \forall x \in \text{range}(E_{a,k}^\top \otimes I_d), \forall t \geq 0. \quad (24)$$

Applying the variation-of-constants formula to (12) over $[t_k, t]$ yields

$$e(t) = e^{-(L_{e,k}^a \otimes I_d)(t-t_k)} e(t_k^+) + \int_{t_k}^t e^{-(L_{e,k}^a \otimes I_d)(t-s)} w(s) ds.$$

Taking norms and using (24) gives (18). If $\|w(s)\| \leq \bar{w}$ on $[t_k, t_{k+1})$, then

$$\int_{t_k}^t e^{-\lambda_k(t-s)} \|w(s)\| ds \leq \bar{w} \int_{t_k}^t e^{-\lambda_k(t-s)} ds = \frac{\bar{w}}{\lambda_k} (1 - e^{-\lambda_k(t-t_k)}),$$

which implies (19).

Step 5: Jump at supervision times. If the radius-induced graph does not change across t_k , then E_k is unchanged and $p(t)$ is continuous while z^r may jump. From (9),

$$e(t_k^+) - e(t_k^-) = (z^r(t_k^+) - z(t_k)) - (z^r(t_k^-) - z(t_k)) = z^r(t_k^+) - z^r(t_k^-) = \Delta z_k^r,$$

which yields (20). If the radius-induced graph changes at t_k , then E_k changes and the post-update error is reinitialized in the new edge coordinates as described earlier; this concludes the proof. \square

We then offer the proof for Corollary 1.

Proof. For any $t \in [t_k, t_{k+1})$, by triangle inequality,

$$\|z(t) - z^*(t)\| \leq \|z(t) - z^r(t)\| + \|z^r(t) - z^*(t)\| = \|e(t)\| + \|z^r(t) - z^*(t)\|.$$

By the assumed grounding bound, $\|z^r(t) - z^*(t)\| \leq \varepsilon_z$. By (19) with $\|w(t)\| \leq \bar{w}$,

$$\|e(t_{k+1}^-)\| \leq e^{-\lambda_k \Delta} \|e(t_k^+)\| + \frac{\bar{w}}{\lambda_k} (1 - e^{-\lambda_k \Delta}).$$

Thus

$$\|z(t_{k+1}^-) - z^*(t_{k+1}^-)\| \leq e^{-\lambda_k \Delta} \|e(t_k^+)\| + \frac{\bar{w}}{\lambda_k} (1 - e^{-\lambda_k \Delta}) + \varepsilon_z.$$

Requiring the right-hand side to be $\leq \delta_z$ and rearranging yields exactly $\|e(t_k^+)\| \leq \eta_{\max}^{(z)}(\delta_z, \Delta, \varepsilon_z)$. \square

D Horizon-wide error bounds under stochastic LLM verification

Recall that $z^*(t)$ denotes the *ground-truth* edge-relative reference consistent with the human intent. Define the ground-truth edge error

$$e_{\text{gt}}(t) := z(t) - z^*(t).$$

Then, for all t ,

$$\|e_{\text{gt}}(t)\| \leq \|e(t)\| + \|z^r(t) - z^*(t)\|. \quad (25)$$

We extend Assumption 1 to a long horizon.

Assumption 2. (B1) **Relative reference held between checks.** Assumption 1(A1) holds on all intervals $[t_k, t_{k+1})$.

(B2) **Uniform contraction.** The neighbor graph does not change across any t_k and

$$\|z^r(t_k^+) - z^r(t_k^-)\| \leq \bar{J}_z, \quad \forall k,$$

for some $\bar{J}_z < \infty$. Since the incidence matrix E_k and edge Laplacian $L_{e,k}^a$ will stay constant, we can denote $\underline{\lambda} = \lambda_k$ for all k .

(B3) **Bounded specification gap in relative coordinates.** There exist $0 \leq \varepsilon_C \leq \varepsilon_W < \infty$ such that, for all k ,

$$\sup_{t \in [t_k, t_{k+1})} \|z^r(t) - z^*(t)\| \leq \begin{cases} \varepsilon_C, & S_k = C, \\ \varepsilon_W, & S_k = W. \end{cases}$$

The above assumption holds when the user's intention does not change in the time horizon, and the environment does not change rapidly. In this case, the formation of the drones will stay relatively consistent throughout the entire time horizon, and the neighbor relationship will also remain constant. When the user's intention changes or the environment changes rapidly, the formation of the drones will be significantly impacted, making the total error difficult to bound. For example, if the original user intention is to form a grid around a target, and then the user decides to form a circle around another target very far away, the error incurred in this process will significantly impact the final regret bound. Assumption 2 is to prevent this from happening.

Theorem 2 (Horizon-wide relative tracking bound under stochastic LLM verification). *Under Assumption 2, define $\eta_k := \|e(t_k^+)\|$ and $\alpha := e^{-\underline{\lambda}\Delta_t}$. Let $\bar{w} := \sup_t \|(E_k^\top \otimes I_d)d(t)\|$ on each interval; under (B1)–(B2) one may take $\bar{w} \leq \|E_k^\top \otimes I_d\|\bar{d}$ to be a constant. Then:*

(i) **Uniform bound on edge tracking to the enforced relative reference.** For all $k \geq 0$,

$$\eta_{k+1} \leq \alpha \eta_k + \frac{\bar{w}}{\underline{\lambda}}(1 - \alpha) + \bar{J}_z. \quad (26)$$

Hence

$$\eta_k \leq \alpha^k \eta_0 + \left(1 - \alpha^k\right) \left(\frac{\bar{w}}{\underline{\lambda}} + \frac{\bar{J}_z}{1 - \alpha} \right), \quad (27)$$

and for any $t \in [t_k, t_{k+1})$,

$$\|e(t)\| \leq e^{-\underline{\lambda}(t-t_k)} \eta_k + \frac{\bar{w}}{\underline{\lambda}} \left(1 - e^{-\underline{\lambda}(t-t_k)}\right). \quad (28)$$

(ii) **Expected ground-truth relative error over a finite horizon.** For $K \geq 1$ and horizon $T_f = K\Delta_t$,

$$\frac{1}{T_f} \int_0^{T_f} \mathbb{E}\|e_{\text{gt}}(t)\| dt \leq \underbrace{\frac{\bar{w}}{\underline{\lambda}} + \frac{\bar{J}_z}{\underline{\lambda}\Delta_t}}_{\text{tracking-to-LLM term}} + \underbrace{\varepsilon_C + (\varepsilon_W - \varepsilon_C) \cdot \frac{1}{K} \sum_{k=0}^{K-1} p_k + \frac{\max\{0, \eta_0 - \eta_\infty\}}{K \underline{\lambda} \Delta_t}}_{\text{specification-gap term}}, \quad (29)$$

where $\eta_\infty := \frac{\bar{w}}{\lambda} + \frac{\bar{J}_z}{1-e^{-\lambda\Delta t}}$ and $p_k = \mathbb{P}(S_k = \mathbb{W})$.

Moreover, for the two-state chain in this section,

$$p_k = \pi_{\mathbb{W}} + (p_0 - \pi_{\mathbb{W}})(1 - a - b)^k, \quad \frac{1}{K} \sum_{k=0}^{K-1} p_k = \pi_{\mathbb{W}} + (p_0 - \pi_{\mathbb{W}}) \frac{1 - (1 - a - b)^K}{K(a + b)}.$$

(iii) **Long-run average bound.** As $T_f \rightarrow \infty$,

$$\limsup_{T_f \rightarrow \infty} \frac{1}{T_f} \int_0^{T_f} \mathbb{E} \|e_{\text{gt}}(t)\| dt \leq \frac{\bar{w}}{\lambda} + \frac{\bar{J}_z}{\lambda \Delta t} + \varepsilon_{\mathbb{C}} + \pi_{\mathbb{W}} (\varepsilon_{\mathbb{W}} - \varepsilon_{\mathbb{C}}). \quad (30)$$

Proof.

Step 1: Bounding $w(t)$ under a relative hold. Under Assumption 2 (B1), $\dot{z}^r(t) = 0$ on $[t_k, t_{k+1})$, hence by (14), $w(t) = -(E_k^\top \otimes I_d)d(t)$ and thus $\|w(t)\| \leq \bar{w}$ on the interval.

Step 2: One-interval ISS bound and the discrete recursion. Given (19) and Assumption 2 (B2), we have

$$\|e(t)\| \leq e^{-\lambda(t-t_k)} \|e(t_k^+)\| + \frac{\bar{w}}{\lambda} (1 - e^{-\lambda(t-t_k)}),$$

which is (28). Evaluating at $t = t_{k+1}^-$ gives

$$\|e(t_{k+1}^-)\| \leq \alpha \eta_k + \frac{\bar{w}}{\lambda} (1 - \alpha).$$

Assumption 2 (B2) and (20) implies $e(t_{k+1}^+) = e(t_{k+1}^-) + \Delta z_{k+1}^r$ with $\Delta z_{k+1}^r := z^r(t_{k+1}^+) - z^r(t_{k+1}^-)$, hence

$$\eta_{k+1} = \|e(t_{k+1}^+)\| \leq \|e(t_{k+1}^-)\| + \|\Delta z_{k+1}^r\| \leq \alpha \eta_k + \frac{\bar{w}}{\lambda} (1 - \alpha) + \bar{J}_z,$$

which is (26). Unrolling (26) yields (27) exactly as for a scalar affine contraction.

Step 3: Finite-horizon average bound. From (25) and Tonelli's theorem,

$$\frac{1}{T_f} \int_0^{T_f} \mathbb{E} \|e_{\text{gt}}(t)\| dt \leq \underbrace{\frac{1}{T_f} \int_0^{T_f} \mathbb{E} \|e(t)\| dt}_{(I)} + \underbrace{\frac{1}{T_f} \int_0^{T_f} \mathbb{E} \|z^r(t) - z^*(t)\| dt}_{(II)}.$$

Term (II). By Assumption 2 (B3), for all $t \in [t_k, t_{k+1})$, $\|z^r(t) - z^*(t)\| \leq \varepsilon_{\mathbb{C}} \mathbf{1}_{\{S_k = \mathbb{C}\}} + \varepsilon_{\mathbb{W}} \mathbf{1}_{\{S_k = \mathbb{W}\}}$. Taking expectation gives $\mathbb{E} \|z^r(t) - z^*(t)\| \leq \varepsilon_{\mathbb{C}} + (\varepsilon_{\mathbb{W}} - \varepsilon_{\mathbb{C}}) p_k$, and integrating over $[0, T_f]$ yields the specification-gap term in (29).

Term (I). The bound (28) implies, for $t \in [t_k, t_{k+1})$,

$$\|e(t)\| \leq \frac{\bar{w}}{\lambda} + e^{-\lambda(t-t_k)} \left(\eta_k - \frac{\bar{w}}{\lambda} \right)_+.$$

Term (I). Fix $k \in \{0, \dots, K-1\}$ and consider $t \in [t_k, t_{k+1})$. Starting from (28) and rearranging,

$$\begin{aligned} \|e(t)\| &\leq e^{-\lambda(t-t_k)} \eta_k + \frac{\bar{w}}{\lambda} (1 - e^{-\lambda(t-t_k)}) \\ &= \frac{\bar{w}}{\lambda} + e^{-\lambda(t-t_k)} \left(\eta_k - \frac{\bar{w}}{\lambda} \right) \\ &\leq \frac{\bar{w}}{\lambda} + e^{-\lambda(t-t_k)} \left(\eta_k - \frac{\bar{w}}{\lambda} \right)_+. \end{aligned} \quad (31)$$

Integrating (31) over $[t_k, t_{k+1})$ and using $\int_{t_k}^{t_{k+1}} e^{-\lambda(t-t_k)} dt = \int_0^\Delta e^{-\lambda s} ds = \frac{1-e^{-\lambda\Delta}}{\lambda}$ yields the *pathwise* bound

$$\int_{t_k}^{t_{k+1}} \|e(t)\| dt \leq \Delta \frac{\bar{w}}{\lambda} + \frac{1-\alpha}{\lambda} \left(\eta_k - \frac{\bar{w}}{\lambda} \right)_+, \quad \alpha := e^{-\lambda\Delta}. \quad (32)$$

Summing (32) over $k = 0, \dots, K-1$, dividing by $T_f = K\Delta$, and taking expectations gives

$$(I) = \frac{1}{T_f} \int_0^{T_f} \mathbb{E} \|e(t)\| dt \leq \frac{\bar{w}}{\lambda} + \frac{1-\alpha}{\lambda\Delta} \cdot \frac{1}{K} \sum_{k=0}^{K-1} \mathbb{E} \left[\left(\eta_k - \frac{\bar{w}}{\lambda} \right)_+ \right]. \quad (33)$$

It remains to upper bound the average of the positive parts. Define the shifted nonnegative sequence

$$\xi_k := \left(\eta_k - \frac{\bar{w}}{\lambda} \right)_+.$$

From the recursion (26),

$$\eta_{k+1} \leq \alpha \eta_k + \frac{\bar{w}}{\lambda} (1-\alpha) + \bar{J}_z,$$

subtracting \bar{w}/λ from both sides gives

$$\eta_{k+1} - \frac{\bar{w}}{\lambda} \leq \alpha \left(\eta_k - \frac{\bar{w}}{\lambda} \right) + \bar{J}_z. \quad (34)$$

Taking positive parts on both sides and using $(\alpha x + \bar{J}_z)_+ \leq \alpha x_+ + \bar{J}_z$ for $\alpha \in [0, 1]$ and $\bar{J}_z \geq 0$ yields the *nonnegative affine recursion*

$$\xi_{k+1} \leq \alpha \xi_k + \bar{J}_z. \quad (35)$$

Unrolling (35) gives, for all $k \geq 0$,

$$\xi_k \leq \alpha^k \xi_0 + \bar{J}_z \sum_{i=0}^{k-1} \alpha^i = \alpha^k \xi_0 + \frac{\bar{J}_z}{1-\alpha} (1-\alpha^k). \quad (36)$$

Averaging (36) over $k = 0, \dots, K-1$ and using $\frac{1}{K} \sum_{k=0}^{K-1} \alpha^k = \frac{1-\alpha^K}{K(1-\alpha)}$ yields

$$\begin{aligned} \frac{1}{K} \sum_{k=0}^{K-1} \xi_k &\leq \frac{\bar{J}_z}{1-\alpha} + \left(\xi_0 - \frac{\bar{J}_z}{1-\alpha} \right) \frac{1-\alpha^K}{K(1-\alpha)} \\ &\leq \frac{\bar{J}_z}{1-\alpha} + \left(\xi_0 - \frac{\bar{J}_z}{1-\alpha} \right)_+ \frac{1-\alpha^K}{K(1-\alpha)} \leq \frac{\bar{J}_z}{1-\alpha} + \frac{1}{K(1-\alpha)} \left(\xi_0 - \frac{\bar{J}_z}{1-\alpha} \right)_+. \end{aligned} \quad (37)$$

Taking expectations in (37) preserves the inequality. Substituting (37) into (33) gives

$$(I) \leq \frac{\bar{w}}{\lambda} + \frac{1-\alpha}{\lambda\Delta} \left(\frac{\bar{J}_z}{1-\alpha} + \frac{1}{K(1-\alpha)} \left(\xi_0 - \frac{\bar{J}_z}{1-\alpha} \right)_+ \right) = \frac{\bar{w}}{\lambda} + \frac{\bar{J}_z}{\lambda\Delta} + \frac{1}{K\lambda\Delta} \left(\xi_0 - \frac{\bar{J}_z}{1-\alpha} \right)_+. \quad (38)$$

Finally, since $\xi_0 = (\eta_0 - \bar{w}/\lambda)_+$ and $\bar{J}_z/(1-\alpha) \geq 0$, one has the identity

$$\left(\xi_0 - \frac{\bar{J}_z}{1-\alpha} \right)_+ = \left(\eta_0 - \frac{\bar{w}}{\lambda} - \frac{\bar{J}_z}{1-\alpha} \right)_+.$$

With $\eta_\infty := \frac{\bar{w}}{\lambda} + \frac{\bar{J}_z}{1-\alpha} = \frac{\bar{w}}{\lambda} + \frac{\bar{J}_z}{1-e^{-\lambda\Delta}}$, this becomes $(\eta_0 - \eta_\infty)_+$, and (38) matches the tracking term used in (29).

Combining (I) and (II) yields (29).

Finally, the closed form for p_k and $\frac{1}{K} \sum_{k=0}^{K-1} p_k$ follows from the scalar recursion $p_{k+1} = a + (1-a-b)p_k$.

Step 4: Long-run bound. Since $|1-a-b| < 1$, we have $\frac{1}{K} \sum_{k=0}^{K-1} p_k \rightarrow \pi_W$ and $\frac{(\eta_0 - \eta_\infty)_+}{K\lambda\Delta} \rightarrow 0$ as $K \rightarrow \infty$. Taking \limsup in (29) yields (30). \square